Enhancement of the reflectivity of soft-x-ray Co/C multilayers at grazing incidence by thermal treatment

1996 J. Phys.: Condens. Matter 8 8763

(http://iopscience.iop.org/0953-8984/8/45/012)

J. Phys.: Condens. Matter **8** (1996) 8763–8776. Printed in the UK

Enhancement of the reflectivity of soft-x-ray Co/C multilayers at grazing incidence by thermal treatment

H L Bai, E Y Jiang, C D Wang and R Y Tian

Department of Applied Physics, Tianjin University, Tianjin 300072, People's Republic of China

Received 14 May 1996, in final form 5 July 1996

Abstract. We report a significant increase in the reflectivity of a soft x-ray Co/C multilayer at grazing incidence after low-temperature annealing. By monitoring the enhancement of the first-order modulation peak on annealing, an effective interdiffusion coefficient as low as -10^{-25} m^2 s^{-1} has been measured, which is nearly equal to the true macroscopic interdiffusion coefficient as the modulation wavelength of the Co/C multilayer studied is well above the critical wavelength. The *negative* true macroscopic interdiffusion coefficient indicates that there is a tendency to phase separation in the Co–C system, which can be interpreted as the positive enthalpy of mixing calculated on the basis of Miedema's macroscopic atom model. The decrease in reflectivity above some annealing temperature is also discussed and explained as the competition between interfacial sharpness and roughness. This is the first report of observations of enhanced reflectivity in the Co/C multilayered system.

1. Introduction

The soft-x-ray multilayer is an alternately layered structure consisting of two materials of different scattering powers at x-ray wavelengths [1]. The multilayer is useful in making reflective components for soft-x-ray regions, since no single material has a significant reflectance at these wavelengths. The reflectivity of a multilayer depends sensitively on the structures of the constituents and the interfaces between them [2–4]. The three principal features which determine the reflectivity of an x-ray multilayer are interfacial roughness, interdiffusion and optical contrast between the constituting materials. During annealing, the crystallization of the amorphous constituents (if they are amorphous) [5, 6], the formation of intermetallic compounds [7, 8], the interdiffusion between layers [9, 10], and the changes in layer roughness [11, 12] each contribute to altering the reflective performance of the multilayer as a reflecting mirror. As such, the mechanisms causing the changes in reflectivity during annealing need to be clarified.

The increase in the reflectivity on annealing was noted by Barbee [13] and Kortright *et al* [14] for W/C multilayers, and the increase was suggested to have resulted from the increased lateral uniformity in the layered structure and/or from the sharper concentration gradient across the interfaces. Generally speaking, several features are responsible for the increase in reflectivity:

(1) the expansion of spacer layers [15–17];
(2) the increase in optical contrast between the constituting materials [18];
(3) the sharpening of the interfaces [9, 13, 14];
(4) the improvement in lateral uniformity [13, 14].

0953-8984/96/458763+14$19.50

As effective soft-x-ray mirrors, Co/C multilayers have been successfully used in an x-ray telescope [19–21]. This paper reports the first observation of enhanced reflectivity at grazing incidence in a Co/C multilayer system by low-temperature annealing. The mechanism of the change in reflectivity at high temperatures is also discussed. We have used small-angle x-ray diffraction with a wavelength of 0.154 05 nm to investigate the reflective properties. The measurements at shorter x-ray wavelengths are preferred to those at longer wavelengths for characterization of the quality of a multilayer for several reasons [22]:

(1) Reflectometers for these wavelengths are available in most laboratories.

(2) The optical constants of materials are better known and more reliable.

(3) Reflectivity can be obtained over a large range of incidence angles and with a large dynamic range.

(4) Once a multilayer has been fully characterized at $\lambda = 0.154\,05$ nm, the possible performance at longer wavelengths can be predicted with the optical constants defining most of the possible errors in this prediction.

2. Experimental details

2.1. Multilayer fabrication

The multilayer samples were made by a dual-facing-target sputtering system. The typical base pressure of the chamber was below 1×10^{-6} Torr. The targets 10 cm in diameter were 99.99% pure Co and 99.999% pure C. During the deposition, the pressure of Ar gas was kept at 4.0×10^{-3} Torr. Typical deposition rates were 0.03 nm s^{-1} for cobalt and 0.01 nm s^{-1} for carbon. The sublayer thickness was monitored with a quartz crystal oscillator. Layering is accomplished by the sequential rotation of the substrate over pure Co and C sputter sources. A series of Co/C multilayers were fabricated on ultra-smooth crystalline ⟨111⟩ silicon wafers and NaCl crystals with a freshly cleaved surface. No attempt was made to remove the natural oxide layer on the silicon wafers prior to the deposition. Each multilayer begins with a C layer and ends also with a C layer, and the thickness of the last C layer is twice those of the other sublayers in order to retard oxidation. The nominal structure has a period of 5.0 nm, with a Γ ratio of the thickness of the Co layer to the multilayer period of 0.4. The temperature inside the chamber during the deposition was below 100 °C. No attempt was made to control the substrate temperature throughout the deposition.

2.2. Annealing treatment

Classical annealing was performed in a furnace at 10^{-6} Torr pressure. The temperature was measured with a (Ni–Cr)–(Ni–Al) thermocouple and controlled to within ± 1 K. After each treatment and prior to performing reflectivity measurements the samples were cooled to room temperature before being taken out of the vacuum chamber. The time for anneals was corrected by taking into account the heating and cooling times. Different annealing temperatures and durations were selected for various annealing treatments. To prevent sample-to-sample fluctuation, the same sample was cut into pieces with the same shape and area, and each piece was characterized before and after the treatment.

2.3. Sample characterization

2.3.1. Small-angle x-ray diffraction. All x-ray diffraction was made using the Cu Kα lines with a wavelength $\lambda = 0.154\,05$ nm. The multilayer period Λ was calculated from the

Bragg equation, modified for refraction [23], given by

$$\sin^2\theta_m = \left(\frac{m\lambda}{2\Lambda}\right)^2 + 2\delta \tag{1}$$

where Λ is the modulation period, m the integer reflection order number and δ the average deviation of the refractive index from unity. Using equation (1) Λ and δ can be determined from the linear regression of $\sin^2\theta_m$ versus m^2 plots. The relation between the average Co concentration and refractive index for Co/C multilayers is given by

$$\delta = c\delta_{Co} + (1-c)\delta_c \tag{2}$$

where c is the Co atomic fraction. The x-ray refractive index δ_j, j = Co or C, for the jth atomic constituent of the multilayer can be obtained from the atomic scattering factors [24]

$$\delta_j = \frac{\lambda^2 r_e N_j}{2\pi}(f_j + \Delta f_j' + \mathrm{i}\Delta f_j'') \tag{3}$$

where r_e is the classical electron radius, N_j the atomic number density and f_j the atomic scattering factor. $\Delta f_j'$ and $\Delta f_j''$ are the real and imaginary corrections, respectively, to f_j due to the presence of absorption edges. The values of $\Delta f_j'$ and $\Delta f_j''$ can be obtained from [25]. By using equations (1)–(3), the average Co concentration of the multilayer can be calculated.

2.3.2. Large-angle x-ray diffraction. Large-angle x-ray diffraction is a well established technique for determining the crystal structure of thin films. The measurement provides information about the composition and average size of crystallites in the direction of momentum transfer of the x-rays. Standard θ–2θ large-angle x-ray diffraction was used here to identify the phase presented in the Co/C multilayers.

2.3.3. Transmission electron microscopy. The samples deposited on the NaCl(100) single-crystal were examined using a JEM-200 CX transmission electron microscope operated at 200 kV. Selected-area electron diffraction was employed to characterize the films at various annealing temperatures.

Selected-area electron diffraction and large-angle x-ray diffraction both provide information about the phases present, but the former is more powerful for phase identification since, in our case, the electrons have a much shorter wavelength.

3. Results

3.1. Structure characterization for as-deposited multilayers

Figures 1 and 2(a) show the large-angle x-ray diffraction spectrum, and the selected-area electron diffraction pattern and microstructures, respectively, of as-deposited Co/C multilayers with a nominal period of 5.0 nm, indicating that the as-deposited Co/C multilayers are amorphous. Figure 3 shows the small-angle x-ray diffraction peaks induced from the compositionally modulated structure of the Co/C multilayers with a nominal modulation period of 5.0 nm. The modulation period Λ can be derived from the positions of modulation peaks using the modified Bragg law, i.e. equation (1). Figure 4 shows the plot of $\sin^2\theta_m$ versus m^2. As is expected from equation (1), all the data points fit very well on a straight line, from which Λ and δ are determined. The values of Λ and δ are listed in table 1. By means of equation (3), the 'real parts' of δ_{Co} and δ_C are calculated to be

2.344×10^{-5} and 6.425×10^{-6}, respectively. Fitting the data to equation (2) we obtained the values of c for the Co/C multilayers as presented in table 1. This result was consistent with that obtained from our nominal Γ value of 0.4 where the average composition of the sample was calculated to be $Co_{37}C_{63}$.

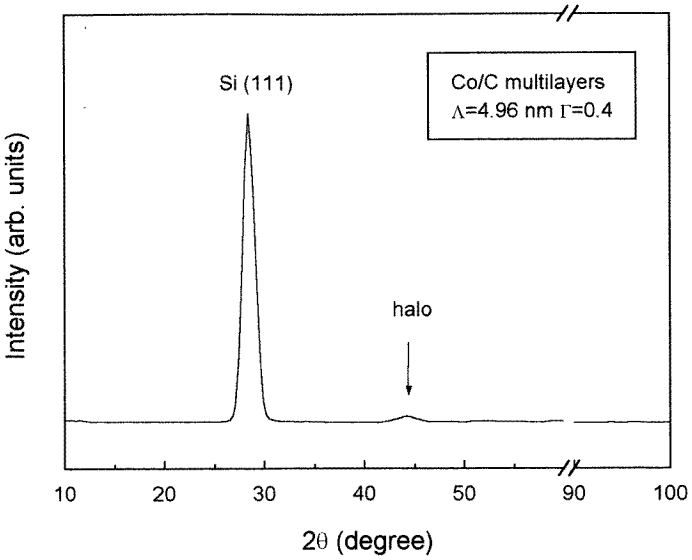

Figure 1. Large-angle x-ray diffraction spectrum for the as-deposited Co/C multilayers of 4.96 nm period.

Table 1. Character of Co/C multilayers: Nom, data obtained from nominal structure; Fit, data obtained from fitting results.

Λ (nm)		δ_a (10^{-5})	c	
Nom	Fit	Fit	Nom	Fit
5.00	4.96	1.289	0.37	0.38

3.2. Annealing time dependence of the reflectivity at grazing incidence

In figure 3, although four modulation peaks are detected, the intensities of second-, third- and fourth-order peaks are much weaker than that of the first-order peak, indicating that the composition profile along the normal to the film plane was close to sinusoidal. If the composition modulation is of small amplitude, it is reasonable to neglect the composition dependence of mobility M, the second derivative f_0'' of the Helmholtz energy and the gradient energy coefficient k. Thus, the amplitude of the composition modulation can be described by Cahn's [26] linear diffusion equation

$$\frac{\partial c}{\partial t} = D\frac{\partial^2 c}{\partial x^2} - \frac{2D}{f_0''}k\frac{\partial^4 c}{\partial x^4} \tag{4}$$

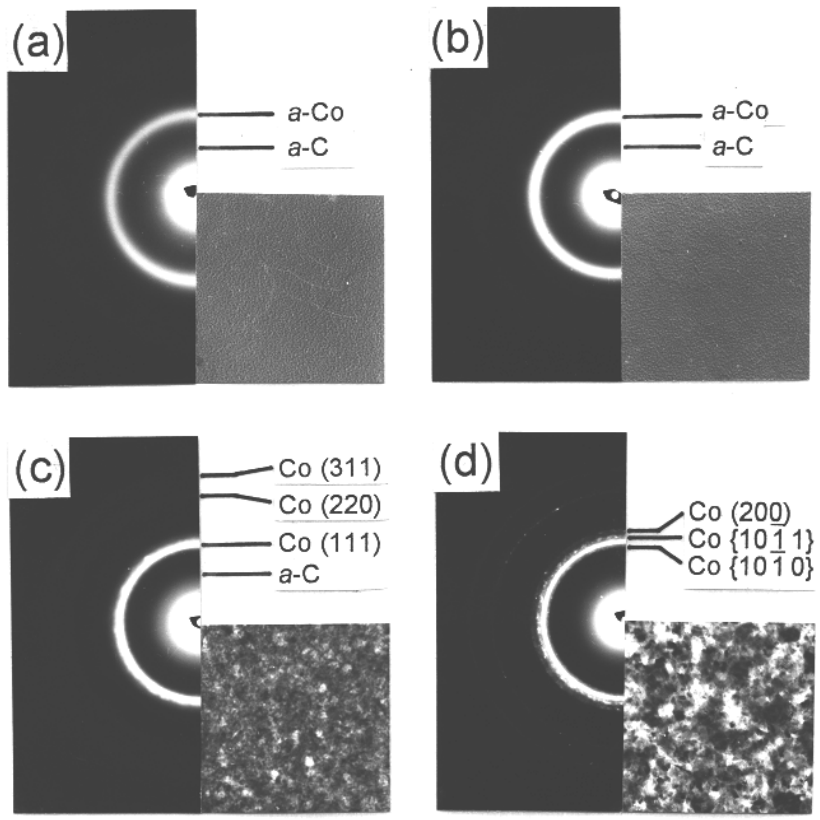

Figure 2. The selected-area electron diffraction patterns and microstructures of the ten-layer pair 4.96 nm Co/C multilayers annealed at different temperatures for 1 h; (a) as deposited; (b) 523 K; (c) 573 K; (d) 673 K.

where c is the atomic fraction of one of components, x a spatial coordinate (normal to the film plane in this case), and D the macroscopic interdiffusion coefficient equal to Mf_0''. A particular solution to equation (1) of interest here is

$$c - c_0 = A(t)\cos(\beta x) \tag{5}$$

$$A(t) = A_0 \exp\left[-D\beta^2\left(1 + \frac{2k\beta^2}{f_0''}\right)t\right] \tag{6}$$

in which $\beta = 2\pi/\Lambda$, c_0 is the atomic fraction of the system if it were homogeneous, $A(t)$ the amplitude of the composition wave at time t. It is apparent from equation (6) that the shorter-wavelength Fourier components diffused out during deposition.

A composition modulation in a planar lattice produces satellites about each Bragg peak. In general, satellites result from modulations in both scattering factor and lattice spacing. In the special case of (000) satellites, the latter contribution is negligible and the diffracted intensity is proportional to the square of the Fourier transform of the composition variation. Thus

$$I \propto |A|^2. \tag{7}$$

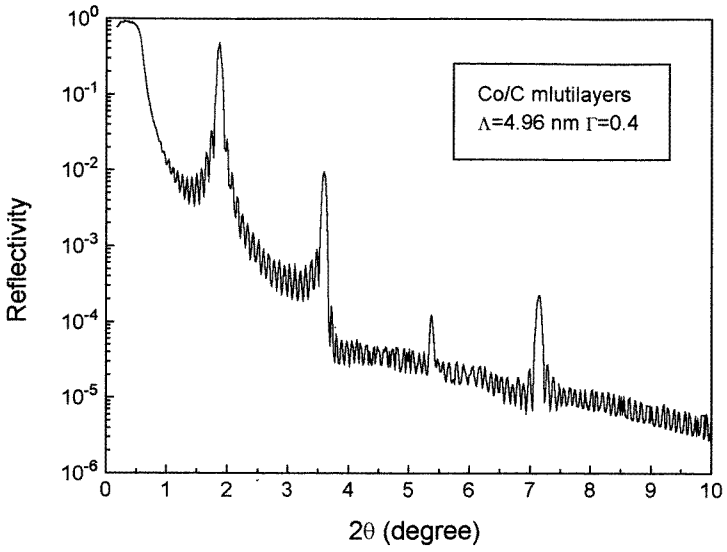

Figure 3. Small-angle x-ray diffraction spectrum of the 20-layer pair Co/C multilayers with periods of 4.96 nm.

From equations (6) and (7), we obtain the time dependence of the intensity of satellites:

$$\frac{\mathrm{d}}{\mathrm{d}t}\left[\ln\left(\frac{I(t)}{I(0)}\right)\right] = -2D\left(1+\frac{2k\beta^2}{f_0''}\right)\beta^2 = -2D_\Lambda\beta^2 \tag{8}$$

where $I(0)$ is the initial intensity and D_Λ is the effective interdiffusion coefficient dependent on the wavelength Λ of the composition modulation under consideration. Substituting β in equation (8) with $2\pi/\Lambda$, we have

$$D_\Lambda = -\frac{\Lambda^2}{8\pi^2}\frac{\mathrm{d}}{\mathrm{d}t}\left[\ln\left(\frac{I(t)}{I(0)}\right)\right]. \tag{9}$$

The intensities $I(t)$ and $I(0)$ of the modulation peak can be either the integrated intensity or the peak intensity. Preliminary measurements revealed that the decay rate of the integrated intensity was the same as that of the peak intensity within experimental error. For convenience, therefore, the latter measurement was used for the estimation of the interdiffusivities here.

Figure 5 shows the changes in the first-order peak intensity with annealing time at three different annealing temperatures. The plots should be linear with a slope proportional to D_Λ if equation (9) is satisfied. It is noted that the enhanced rate of the first-order modulation peak was appreciably faster during the 0–0.5 h anneal, which may be attributed to a decrease in the interfacial short-range disorder. As we know, the as-deposited films should to some degree contain the interfacial disorder which originates in the deposition process, possibly owing to the poor coherency induced by the large difference in the atom size of the constituents. When the temperature is raised, thermal motions are moderately activated, leading to a more regular arrangement of the interfacial atoms and improving lateral uniformity in the layered structures. Accordingly, the short-range disorder is reduced and the reflectivity is then increased. After annealing for 0.5 h, the *isoconfigurational condition* was reached,

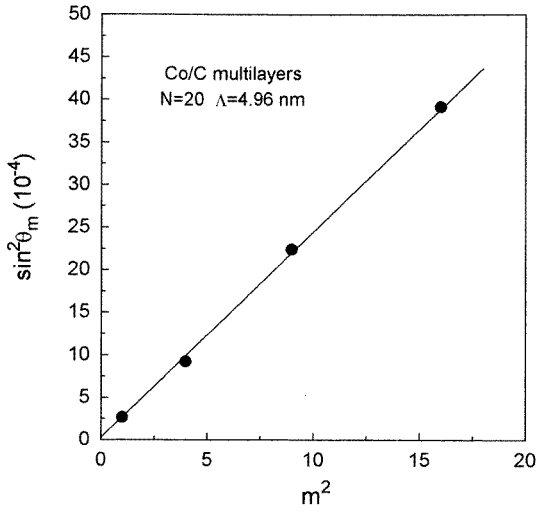

Figure 4. The linear least-squares fits of $\sin^2\theta_m$ versus m^2.

and the variation in $\ln[I(t)/I(0)]$ with t became linear and had a slope characteristic of the interdiffusion process. The effective interdiffusivities can then be obtained by linear least-squares fits, and the results are listed in table 2. The value of the modulation wavelength Λ of the present sample is much larger than the typical critical modulation period of the Co–C system [9]. Thus, the D_Λ obtained is approximately equal to the bulk macroscopic interdiffusion coefficient D (see equation (8)). Noting the values of D_Λ presented in table 2, one can then conclude that the true macroscopic interdiffusion coefficients are negative. This indicates that there is a tendency to phase separation in the Co–C system. This interesting result will be discussed in detail in section 4.

Table 2. The effective interdiffusivities D_Λ for the Co/C multilayers ($\Lambda = 4.96$ nm) at different annealing temperatures.

	D_Λ (10^{-24} m^2 s^{-1})		
Λ (nm)	473 K	498 K	523 K
4.96	−1.009	−5.143	22.420

Another important feature of the enhanced curve at 523 K is non-linearity after annealing for 10 h. This effect should not be attributed to the crystallization and/or grain growth during annealing, because firstly no evidence of crystallization was found through transmission electron microscopy, as shown in figure 2(b) and secondly, for crystallization and grain growth processes, advancing interfaces normal to the substrate would provide high-diffusivity paths, resulting in a larger interdiffusivity. Contrary to this, as indicated in the figure 5, the interdiffusivity after annealing for 10 h was obviously lower than that obtained from the linear regime. We can then interpret the phenomenon as follows. In solving equation (4), it was assumed that D and other coefficients were independent of composition. This assumption is satisfied only in the case when the amplitude of the

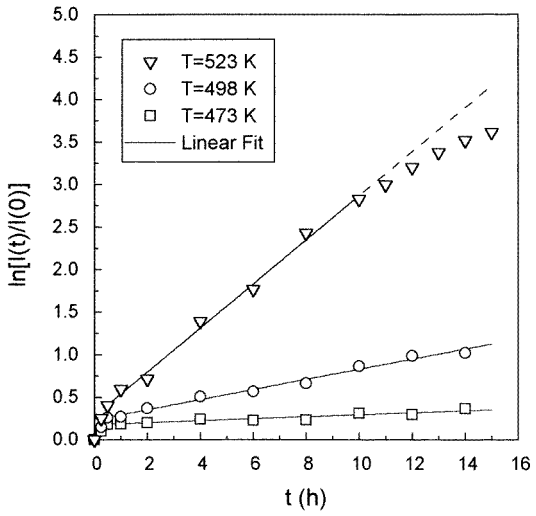

Figure 5. Enhancement of the first-order modulation peak intensity on annealing time and temperature for the Co/C multilayers with periods of 4.96 nm.

composition modulation tends to zero. For a composition modulation of large amplitude such as might arise in the later stages of spinodal decomposition, or in the early stages of annealing an artificially modulated material, the assumption that the mobility M, the second derivative f_0'' of the Helmholtz energy and the gradient energy coefficient k are independent of composition is clearly inadequate, because of the increasing composition gradient. Therefore, the linear diffusion equation (1) is no longer obeyed, and non-linearity appears.

3.3. Annealing temperature dependence of the reflectivity at grazing incidence

A more detailed study of the first- and second-order peak intensities after annealing for 1 h as a function of annealing temperature is displayed in figure 6. The annealing procedure induces significant changes in the reflectivity behaviours, as can be seen in the figure. The first- and second-order Bragg peak intensities have been enhanced considerably at annealing temperatures below 400 °C and 300 °C, respectively. Annealing to 500 °C yields drastic decreases in the intensities of the first- and second-order Bragg peaks. The unusual and significant increase in the intensities, especially in the second-order reflection, results mainly from the structurally sharpened interfaces [11]. The mechanism of the decrease in the first-order (above 300 °C) and the second-order (above 400 °C) Bragg intensities is more complicated owing to the crystallization of amorphous cobalt, as shown in figures 2(c)–(d). Detailed analyses will be carried out in section 4.

4. Discussion

In this section, the mechanisms which result in the enhancement and decay of the grazing-incidence reflectivity will be discussed in detail.

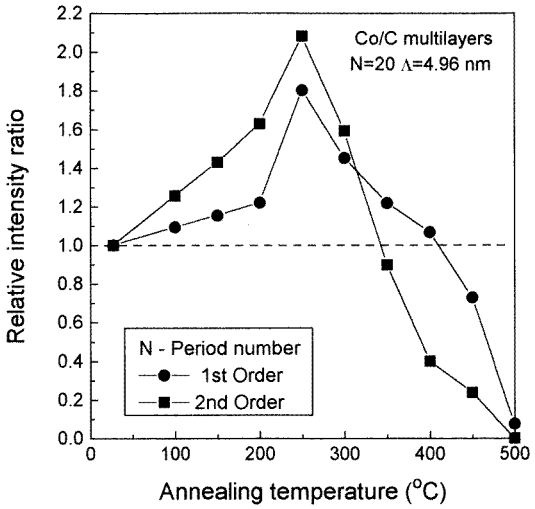

Figure 6. The first- and second-order Bragg maxima intensities after annealing for 1 h relative to the intensity of as-deposited multilayers versus annealing temperature.

4.1. Co–C system phase separation or not

In section 3.2, the result of interdiffusivities measurement indicates the tendency of phase separation in the Co–C system. Now, on the basis of Miedema's macroscopic atom model, we shall calculate the enthalpy ΔH of Co–C mixing to demonstrate our results.

ΔH can be evaluated according to the 'macroscopic atom' model [27] which has been developed to calculate the enthalpy values for binary metal alloys. For Co–C solution, the enthalpy change can be expressed mathematically as

$$\Delta H = \frac{2Pf(c^s)(c_C V_C^{2/3} + c_{Co} V_{Co}^{2/3})}{(n_{WS}^C)^{-1/3} + (n_{WS}^{Co})^{-1/3}} \left(-(\Delta\phi^*)^2 + \frac{Q}{P}(\Delta n_{WS}^{1/3})^2 - \frac{R}{P} \right) + c_C[\Delta H(C_{element} \rightarrow C_{metal})] \tag{10}$$

where

$$f(c^s) = c_C^s c_{Co}^s$$
$$c_C^s = c_C V_C^{2/3}/(c_C V_C^{2/3} + c_{Co} V_{Co}^{2/3})$$
$$c_{Co}^s = c_{Co} V_{Co}^{2/3}/(c_C V_C^{2/3} + c_{Co} V_{Co}^{2/3})$$
$$P = 12.3 \qquad Q/P = 9.4 \text{ V}^2 \text{ (d.u.)}^{2/3} \qquad R/P = 2.1 \text{ V}^2.$$

Here, c_C and c_{Co} are molar concentrations. V_C and V_{Co} are the molar volumes of carbon and cobalt, respectively. ϕ^* is a modified work function and n_{WS} the electron density at the first Wigner–Seitz boundary. P, Q and R are constants. ΔH is expressed in kilojoules per mole, ϕ^* in volts, n_{WS} in density units (d.u.), and $V_C^{2/3}$ and $V_{Co}^{2/3}$ in square centimetres. In equation (10), the first term, which is negative, is proportional to the square of the difference in the electronegativity parameter ϕ^* and therefore the charge transfer between cobalt and carbon. The second term, which is positive, represents the discontinuity in electron density at the Wigner–Seitz boundary of cobalt and carbon atoms. The third term, which is negative,

represents a hybridization contribution. Both the first and the third terms favour a tendency for compound formation, while the second term favours a tendency for phase separation. The last is a transformation energy that accounts for the enthalpy difference between elementary and metallic carbon. According to the theory of Miedema [28], alloys of transition metals with C can be treated as the other alloys of transition metals with polyvalent non-transition metals. The only difference is to introduce an additional *positive* contribution to account for the enthalpy difference between carbon in the diamond structure and a more conventional metallic structure. For carbon, the corresponding transformation energy equals the heat of fusion, 100 kJ mol^{-1}. To improve the agreement between predicted and experimental values, the transformation energy has been changed to 180 kJ mol^{-1} [29].

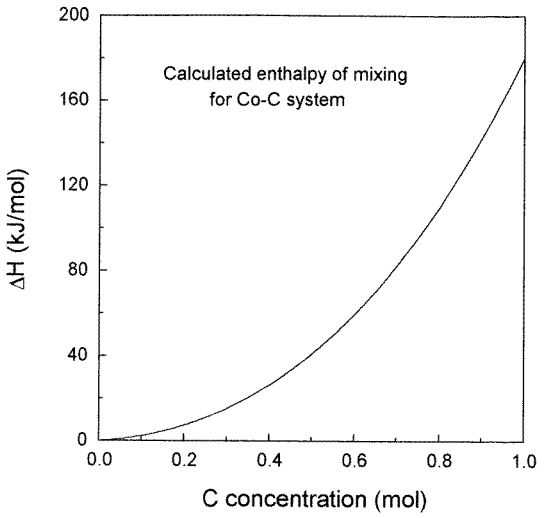

Figure 7. Theoretical calculated enthalpy of mixing for the Co–C system.

The difference $\Delta\phi^*$ in the electronegativities can make a considerable change in the volume of the metal atoms due to the charge transfer effect. Since the value of ϕ^* for carbon is the second highest (the highest is nitrogen) of all metals, the charge transfer effect can be relatively large. An approximate expression for volume changes has been suggested [28] to be

$$(V_A^{2/3})_{alloy} = (V_A^{2/3})_{pure}[1 - ac_A(\phi_A^* - \phi_B^*)] \tag{11}$$

where a is a constant equal to 0.04 for carbon and 0.1 for cobalt.

The values of ϕ^*, $n_{WS}^{1/3}$ and $V_m^{2/3}$ used to calculate ΔH are listed in table 3. The calculated enthalpy of mixing versus C composition curve for the Co–C system is shown in figure 7. From the figure, one can see that any concentration of C solubilizing in Co will result in an increase in the enthalpy of mixing, and the enthalpy increases monotonically with increase in C concentration. That is to say, for a Co–C solution, Co–C mixing can only cause an increase in the heat of mixing. According to the regular solution model [30], the gradient energy coefficient $k \propto \Delta H$; we can then obtain $k > 0$. A positive gradient energy coefficient is characteristic of a phase separation system. This positive k indicates that the Co–C system is phase separated. In other words, it is favourable for the system to separate into two phases at low temperatures.

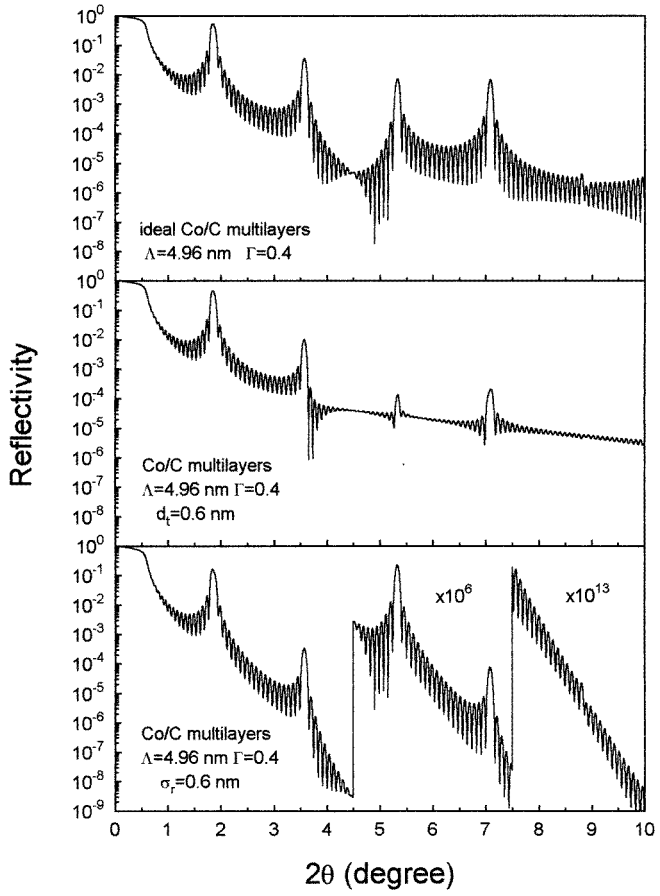

Figure 8. The calculated reflectivity curves for non-ideal Co/C multilayers at grazing incidence.

Table 3. The values of ϕ^*, $n_{WS}^{1/3}$ and $V_m^{2/3}$ for calculating ΔH.

	ϕ^* (V)	$n_{WS}^{1/3}$ ((d.u.)$^{1/3}$)	$V_m^{2/3}$ (cm^{-2})
C	6.24	1.77	2.20
Co	5.10	1.75	3.50

For the binary Co–C alloys, the equilibrium phase diagram indicates that only slight solubility of C (less than 0.4%) in Co matrix can be achieved below 500 °C [31]. However, using the non-equilibrium technique, e.g. sputtering, a metastable Co–C solution with an extended C solubility can be obtained. In our case, a supersaturated Co–C alloy can be achieved at Co–C interfaces during sputtering deposition. Subsequent annealing of the supersaturated Co–C alloy leads to the back interdiffusion of Co and C due to the phase separation. The back interdiffusion results in an increase in composition gradient at interfaces, which is how the reflectivity is increased and accounts for the negative macroscopic interdiffusion coefficient.

4.2. The decrease in the reflectivities of first- and second-order modulation peaks

A very high reflectivity can be predicted for an ideal multilayer structure in the soft-x-ray region [32]. However, achieving the maximum possible reflectivity is often difficult because actual structures can deviate strongly from the ideal model. Although unwanted fluctuations in the layer thickness throughout the multilayer can occur, we assume here that these variations are negligible. The most important deviation is the fact that most interfaces are not atomically sharp but exhibit some kind of roughness or interdiffusion on an atomic scale. These interfacial imperfections will affect the optical performance of the multilayer mirrors and become critically serious as the wavelength of the light is decreased. As an example, interfacial roughness or interdiffusion that blurs the interfaces over a thickness greater than 10% of the wavelength of the light will significantly reduce the performance of the mirrors [33].

Diffusion enhances transmission at the interfaces, reducing reflection, while (owing to absorption) there is no compensating increase in the effective number of layers contributing to reflection. Microroughness at the interfaces causes scattering losses. Since averages over large lateral areas of the sample and projection of the electron density into the direction normal to the surface or interface are taken, neither case can be distinguished by specular reflectivity measurement (θ–2θ) because they exhibit identical electron density gradients. However, the deviation from an abrupt interface affects the scattering vector dependence of the reflectivity, which drops off faster than for an ideally sharp interface. In the case of a roughness interface, the lost intensity is redistributed into the off-specular diffuse region of scattering. In contrast, a diffused interface does not give rise to diffuse scattering. Therefore, the two types of non-ideal interface can only be distinguished by their off-specular diffuse intensity, which can be measured through non-specular x-ray diffraction regimes such as rocking, scattering and offset scans.

If the average *composition gradient* across the layer boundaries is represented by a Gaussian of half-width σ, then the mth-order reflectance R_m will be reduced according to [34]

$$R_m = R_m^0 \exp\left(\frac{-4\pi^2 m^2 \sigma^2}{\Lambda^2}\right) \tag{12}$$

where R_m^0 is the reflectance for the case of an ideal multilayer. It is seen here that imperfect layer boundaries cause the high order of reflection to be preferentially attenuated. Figure 8 gives the calculated reflectivity curves for non-ideal Co/C multilayers at grazing incidence, where we assume that the thickness d_t of the transition layer is equal to the value of RMS roughness σ_r, i.e. $d_t = \sigma_r = 0.6$ nm. Also shown in the figure is the calculated reflectivity curve for ideal Co/C multilayers. From the figure, one can see that the interfacial roughness causes a much stronger decrease in the high orders of reflection. This behaviour can be understood by noting that the number of layers in the multilayers with a transition layer is larger than is required for those with interfacial roughness. A transition layer reduces the reflectivity and increases the transmission at each boundary. As a sequence, the incident light penetrates deeper into the multilayer and is reflected from deeper layers. This reflection compensates partly for the reflection loses at the top boundaries, resulting in a smaller drop in reflectivity.

According to the above discussion, the considerable decrease in the reflectivity of the second-order peak indicates that the reduction is mainly caused by increasing interfacial roughness. From figures 2(c) and (d), we can see that, above 300 °C, the amorphous cobalt crystallizes. Interfacial roughness can thus be significantly increased, causing a

decrease in the reflectivities, especially the second-order reflection. Meanwhile, annealing also results in an interfacial sharpness due to the Co–C phase separation. Therefore, the changes in the reflectivities above 300 °C are the result of competition between interfacial sharpness and roughness. At higher annealing temperatures, the roughness effect becomes more considerable and causes a decrease (the relative intensity ratio is below 1.0 in figure 6) in the reflectivity.

5. Conclusion

We have demonstrated that there is a tendency to phase separation in the Co–C system both theoretically and experimentally. This can give a large increase in the composition gradient at interfaces during annealing, resulting in great enhancement of reflectivity. Our results indicate that low-temperature annealing is an effective method to improve the quality of as-deposited Co–C multilayers. Of course, high-temperature performance should be improved by preventing the amorphous components from crystallization and decreasing the interfacial roughness.

Acknowledgments

This work was financially supported by the National Science Foundation of China and Beijing Zhongguancun Associated Centre of Analysis and Measurement. The authors are grateful to the researchers in the transmission electron microscopy laboratory of Peking University and in the x-ray laboratory of Nankai University for their assistance.

References

[1] Spiller E 1957 *Physics, Fabrication, and Applications of Multilayered Structures* ed P Dhez and C Weisbuch (New York: Plenum) p 271
[2] Stearns D G, Rosen R S and Vernon S P 1991 *J. Vac. Sci. Technol.* A **9** 2662
[3] Slaughter J M, Schulze D W, Hills C R, Mirone A, Stalio R, Watts R N, Tarrio C Lucatorto T B, Krmrey M and Mueller P 1994 *J. Appl. Lett.* **76** 2144
[4] Takenaka H, Kawamura T, Ishil Y and Asagiri S 1995 *J. Appl. Phys.* **78** 5227
[5] Ziegler E, Lepêtre Y, Schuller I K and Spiller E 1986 *Appl. Phys. Lett.* **48** 1354
[6] Lepêtre Y, Ziegler E, Schuller I K and Rivoira R 1986 *J. Appl. Phys.* **64** 2301
[7] Kortright J B and Denlinger J D 1988 *Mater. Res. Soc. Symp. Proc.* vol 103 (Pittsburgh, PA: Materials Research Society) p 95
[8] Stearns D G, Stearns M B, Cheng Y, Stith J H and Ceglio N M 1990 *J. Appl. Phys.* **67** 2415
[9] Bai H L, Jiang E Y and Wang C D 1996 *Thin Solid Films* at press
[10] Nakajima H, Fuhimori H and Koiwa M 1988 *J. Appl. Phys.* **63** 1046
[11] Bai H L, Jiang E Y and Wang C D 1996 *Appl. Phys.* A **63** 57
[12] Stock H-J, Kleineberg U, Heidemann B, Hilgers K, Kloidt A, Schmiedeskamp B, Heinzmann U, Krumrey M, Müller P and Scholze F 1994 *Appl. Phys.* A **58** 371
[13] Barbee T W Jr 1984 *X-ray Microscopy* vol 43, ed G Schmahl and D Rudolph (Berlin: Springer) p 144
[14] Kortright J B, Joksch St and Ziegler E 1991 *J. Appl. Phys.* **69** 168
[15] Jiang X M, Xian D C and Wu Z Q 1990 *Appl. Phys. Lett.* **57** 2549
[16] Jiang Z, Vidal B, Desrousseaux G, Dupuis V, Piecuch M and Ravet M F 1993 *J. Appl. Phys.* **74** 249
[17] Jiang Z, Dupuis V, Vidal B, Ravet M F and Piecuch M 1992 *J. Appl. Phys.* **72** 931
[18] Schlatmann R, Keppel A, Xue Y, Verhoeven J and Van der Wiel M J 1993 *Appl. Phys. Lett.* **63** 3297
[19] Spiller E and Golub L 1989 *Appl. Opt.* **28** 2969
[20] Spiller E, Wilczynski J, Stearns D, Golub L and Nystrom G 1992 *Appl. Phys. Lett.* **61** 1481
[21] Spiller E, Stearns D and Krumrey M 1993 *J. Appl. Phys.* **74** 107
[22] Spiller E and Resenbluth A E 1985 *Proc. SPIE* vol 563 (Bellingham, WA: SPIE) p 221
[23] Agarwal B K 1979 *X-ray Spectroscopy* vol 15 (Berlin: Springer) p 134

[24] Miceli P F, Neumann D A and Zebel H 1986 *Appl. Phys. Lett.* **48** 24
[25] Ibers J A and Hamiton W C (eds) 1974 *International Tables of X-ray Crystallography* (Birmingham: Kyonch) p 149
[26] Cahn T W 1961 *Acta Metall.* **9** 795
[27] Miedema A R, de Châtel P F and de Beer F R 1980 *Physica* B **100** 1
[28] Miedema A R 1976 *J. Less-Common Met.* **46** 67
[29] Niessen A K, Miedema A R, de Beer F R and Boom R 1988 *Physica* B **151** 401
[30] Greer A L and Spaepen F 1985 *Synthetic Modulation Structures* ed L L Chang and B C Giessen (New York: Academic) p 424
[31] Ishida K and Nishizawa T 1991 *J. Phase Equilibria* **12** 417
[32] Rosenbluth A E 1983 *Dissertation* University of Rochester, Rochester, NY
[33] Kearney P A, Slaghter J M and Falco C M 1991 *Opt Eng.* **30** 1076
[34] Stearns D G 1989 *J. Appl. Phys.* **65** 491